

Research Paper

DESIGN AND ANALYSIS OF HIGH SPEED SWITCHED RELUCTANCE MOTOR FOR TWO DIFFERENT MATERIALS

S Rajkumar^{1*}, K Sedhuraman¹, Purimetla Santhi² and A Joycy Faustina Lourdes²

*Corresponding Author: S Rajkumar, ✉ rajkumars4184@gmail.com

In aircraft electric motor driven fuel delivery system, the motor must be characterized by high power density, reliability, less size, less weight and high speed (Radun, 1992). The high speed operation, fault tolerance, high power density makes switched reluctance motor an ideal candidate for high speed aerospace applications. This paper investigates the application potential of soft magnetic composite material (SOMALLOY 500) in high-speed switched reluctance motor. Two configurations: (1) all sheet metal with smooth frame and ribbed frame, (2) all Soft magnetic composite material with smooth frame and ribbed frame have been studied using finite element analysis to obtain their nodal temperature distributions in different parts with two different stator frames such as stator with smooth frame and stator with ribbed frame and mode shapes and mode frequencies. The study reveals that the all soft magnetic composite configuration with ribbed stator frame has a better thermal capability and lesser vibration of stator that may result in low acoustic level a desirable feature in high speed aerospace applications.

Keywords: Finite element analysis, Soft Magnetic Composite (SMC), Switched Reluctance Motor (SRM), Thermal characterization

INTRODUCTION

The low cost, high speed, high power density, fault tolerance and reliability of switched reluctance motor make it a viable alternative in aircraft electric-motor-driven fuel pump system (Radun, 1992). Recently soft magnetic composite materials find rampant applications in electrical machines (Miller, 1993; and

Persson *et al.*, 1995) and these materials are characterized by three-dimensional isotropic ferromagnetic behavior, very low eddy current loss, flexible machine design and assembly and a prospect for greatly reduced production cost.

This paper investigates the application potential of soft magnetic composite material

¹ Department of EEE, Manakula Vinayagar Institute of Technology, Pondicherry, India.

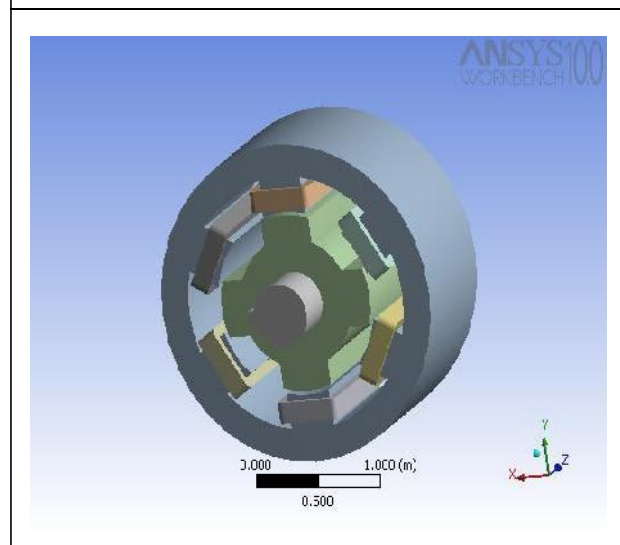
² Department of EEE, Manakula Vinayagar Institute of Technology, Pondicherry, India.

in high-speed switched reluctance motor designed for aerospace applications from a study of its Mechanical behavior. The accurate Result (both thermal and vibration) can be computed in all regions of the machine with two configurations viz., (i) All laminated sheet steels, (ii) All Soft Magnetic Composites (SMC).

The study concludes that all SMCs configuration with ribbed stator frame has better mechanical characteristics.

A switched reluctance motor is an electrical machine in which the torque is developed by the tendency of the rotor to occupy a position so as to minimize the reluctance of the magnetic path of the excited stator phase winding. The switched reluctance motor is a doubly salient but singly excited machine wherein the stator carries the winding while the rotor is simply made of stacked silicon steel laminations. This lends to a simpler geometry for switched reluctance motors as evidenced from the CAD model of a 6/4 switched reluctance motor shown in Figure 1.

Figure 1: CAD Model of 6/4 (3 Phase) SRM

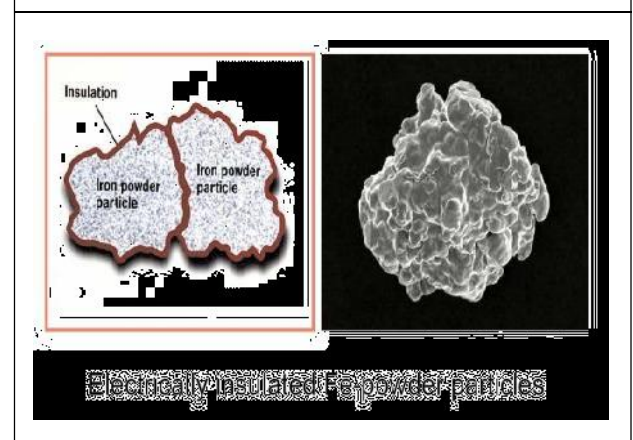


Soft Magnetic Composite Materials in Rotating Electrical Machines

Electrical steel lamination is the most commonly used core material in electrical machines. Electrical steels are typically classified into grain-oriented electrical steels and non-oriented electrical steels. Typical applications for grain-oriented steels are power transformer cores whereas non-oriented steels are broadly used in different kinds of rotating electrical machines. Electromechanical steels currently used in the manufacture of electrical machines possess high induction of magnetic saturation ($B_s \sim 2T$), low coercive force ($H_c < 100 A/m$), and they are characterized by low total losses Miller (1993) and Persson (1995). Electrical sheet steels have been the dominant choice for the soft iron components in electrical machines subject to time varying magnetic fields.

The new soft iron powder metallurgy materials can be considered as an alternative for magnetic core of the electrical machines. The basis for soft magnetic composites is bonded iron powder as shown in Figure 2.

Figure 2: Iron Powder Particle

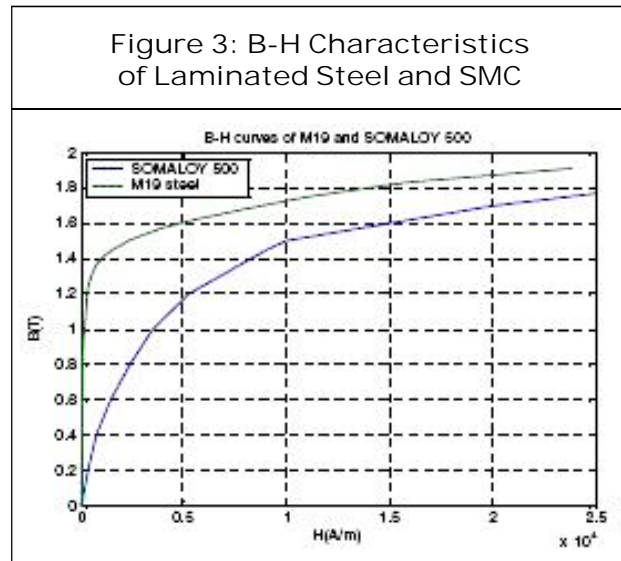


THERMAL ANALYSES

Accurate estimation of losses is a very important issue in the design of high speed and high efficiency motor. In order to estimate the losses and the thermal behaviour of the machine accurately much attention must be paid to the calculation of the losses. The loss components of the machine can be summarized as:

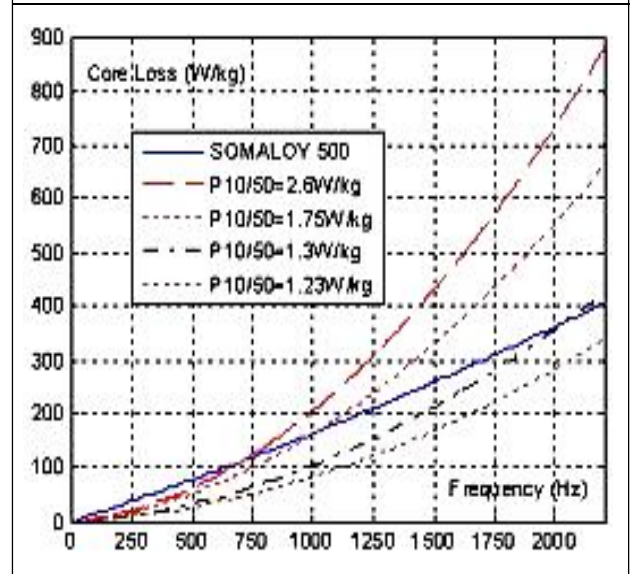
$$P_{loss,m} = P_{cu} + P_{Fe} + P_{mech} \quad \dots(1)$$

The powder is coated, pressed into a solid material using a die, and heat-treated to anneal and cure the bond. The B-H characteristics of M19 silicon steel and SMC material SOMALLOY 500, shown in Figure 3, reveals that although the SMC has inferior relative permeability when compared with lamination steel it still posses the following desirable characteristics (Hogan, 2003).



where P_{cu} , P_{Fe} , P_{mec} are copper losses, core (iron) losses and mechanical loss respectively. These components are successively deal bellow. To estimate the Losses of the complete Switched Reluctance Motor (SRM) to be done. The losses can be estimated based on

Figure 4: Core Losses of SOMALLOY 500



analytical analysis or numerical simulation. The core losses of SOMALLOY 500 characteristics showing in Figure 4.

The heat transferred by radiation is ignored. The partial differential equation of the heat conduction and convection is expressed as:

$$- \{L\} = \begin{Bmatrix} \frac{\partial}{\partial x} \\ \frac{\partial}{\partial y} \\ \frac{\partial}{\partial z} \end{Bmatrix} \{v\} = \begin{Bmatrix} v_x \\ v_y \\ v_z \end{Bmatrix} [D] = \begin{bmatrix} K_{xx} & 0 & 0 \\ 0 & K_{yy} & 0 \\ 0 & 0 & K_{zz} \end{bmatrix} \quad \dots(3)$$

- a. Reduced copper volume as a result of increased fill factor and reduced end winding length and reduced copper loss as a result of the reduced copper volume,

Table 1: Studied Structures	
Configuration-1	Configuration-2
Laminated sheet steel stator (M19)	Soft Magnetic Composite (SMC) stator
Laminated sheet steel rotor (M19)	Soft Magnetic Composite (SMC) rotor

- b. Potential for reduced air gap length as a result of the tight tolerances maintained in manufacturing SMC material,
- c. Modular construction allows the possibility of easy removal of an individual modular unit for quick repair or replacement,
- d. Stator is easily recyclable since the stator can again be compressed back into powered form.

where $[Kg/m]$ is the mass density, $c[J/(KgK)]$ the specific heat, $T[K]$ the temperature, $t[s]$ the time, $\{V\}$ the velocity vector for mass transport of heat, $[D]$ the Thermal conductivity matrix, K_{xx} , K_{yy} , K_{zz} and $K[W/(m \cdot K)]$ are the thermal conductivity along the x, y and z directions, respectively, and $q[W/m]$ is the heat generation rate per unit volume.

For steady-state analysis, the left-hand side term in (2) is zero. This relation is also heat conduction. This differential equation of the heat balance is solved for a finite size of volume whose boundaries specify the heat flow through them.

Boundary Conditions

The boundary conditions can be of Dirichlet type, where the temperature T on the boundary is specified. This boundary condition can be applied to the surface between the frame and outer air. A Neumann type of boundary condition specifies the heat flux flow q_n through the boundary. The heat flux flow through the boundaries to the surrounding is described with the heat transfer coefficient h and the ambient temperature T_{amb} . The governing Equation (4) is given by

$$q_n = n \cdot (k \nabla T) = h(T - T_{amb}) \quad \dots(4)$$

Table 2: Nodal Temperature Differences Between Two Configurations with Smooth Stator Farm		
Material	Minimum Temperature	Maximum Temperature
SMC	316.34	319.04
M19	319.126	321.499
% Difference in Temperature	27.86	24.59

Table 3: Nodal Temperature Differences Between Two Configurations with Ribbed Stator Farm		
Material	Minimum Temperature	Maximum Temperature
SMC	313.383	310.563
M19	314.275	312.445
% Difference in Temperature	27.86	24.59

The convective heat transfer to the surroundings is dependent on the geometry and the cooling conditions. Air gap convection coefficient is determined by two main quantities the ruggedness of the rotor and stator surfaces and the peripheral speed of the rotor surface. By assuming smooth surface, the convection coefficient can be calculated by experiential formula (5) and (6)

$$h_\delta = 28 (1 + \omega_\delta^{0.5})(W/(m^2K)) \quad \dots(5)$$

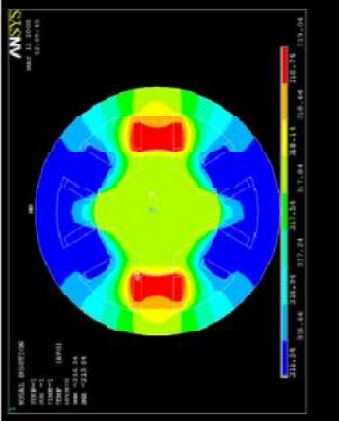
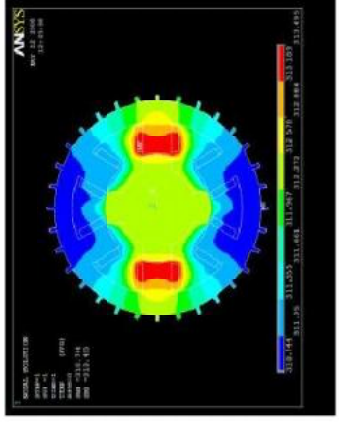
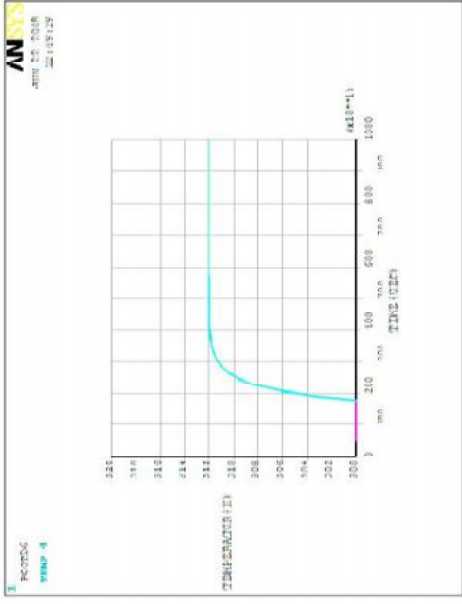
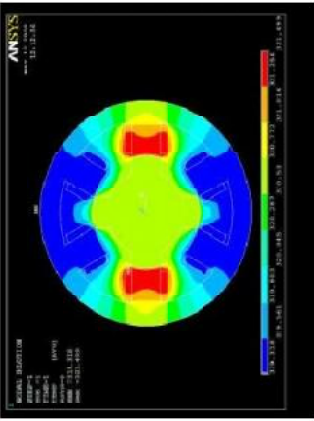
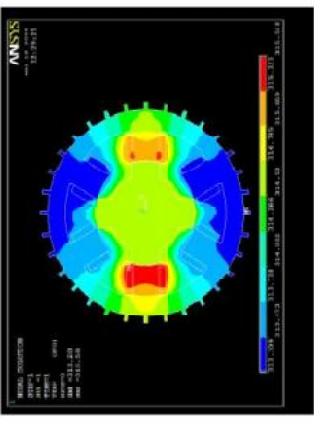
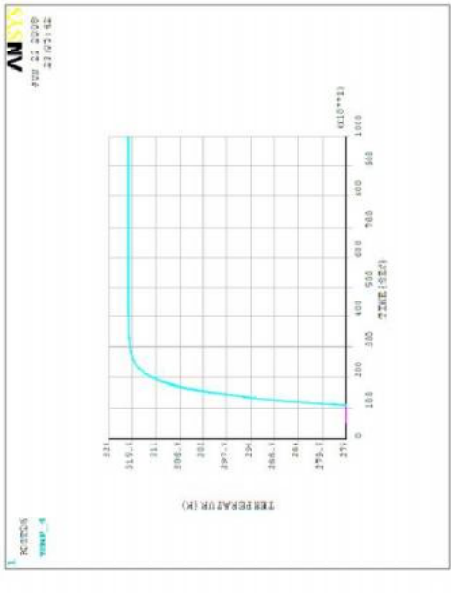
$$\omega_\delta = \{(0.5v_r)^2 + v_a^2 (m/s)\}^{1/2} \quad \dots(6)$$

where v_r and v_a are the peripheral and axial speeds of the rotor surface, respectively:

Transient Thermal Analysis of SRM with SMC and M19

The transient thermal analysis, in which the

Figure 5: Numerical Result of Thermal

 <p>ANSYS 2D nodal temperature plot of smooth frame SMC. The plot shows a circular cross-section with a central hole and four internal ribs. The temperature distribution is color-coded, with the highest temperatures (red) at the inner surfaces of the ribs and the lowest temperatures (blue) at the outer periphery. The color scale ranges from approximately 311.0 to 313.0.</p>	 <p>ANSYS 2D nodal temperature plot of Ribbed frame SMC. The plot shows a circular cross-section with a central hole and four internal ribs. The temperature distribution is color-coded, with the highest temperatures (red) at the inner surfaces of the ribs and the lowest temperatures (blue) at the outer periphery. The color scale ranges from approximately 311.0 to 313.0.</p>	 <p>ANSYS graph showing the 2D nodal temperature of SMC versus Time (SEC). The temperature starts at approximately 302.5 and rises sharply to about 311.5 within the first 100 seconds, then continues to rise more gradually, reaching a steady state of approximately 312.5 after 1000 seconds.</p>
 <p>ANSYS 2D nodal temperature plot of smooth frame M19. The plot shows a circular cross-section with a central hole and four internal ribs. The temperature distribution is color-coded, with the highest temperatures (red) at the inner surfaces of the ribs and the lowest temperatures (blue) at the outer periphery. The color scale ranges from approximately 311.0 to 313.0.</p>	 <p>ANSYS 2D nodal temperature plot of Ribbed frame M19. The plot shows a circular cross-section with a central hole and four internal ribs. The temperature distribution is color-coded, with the highest temperatures (red) at the inner surfaces of the ribs and the lowest temperatures (blue) at the outer periphery. The color scale ranges from approximately 311.0 to 313.0.</p>	 <p>ANSYS graph showing the 2D nodal temperature of M19 versus Time (SEC). The temperature starts at approximately 302.5 and rises sharply to about 311.5 within the first 100 seconds, then continues to rise more gradually, reaching a steady state of approximately 312.5 after 1000 seconds.</p>

temperature varies with respect to time, is stimulated for continuous duty cycle.

VIBRATION ANALYSES

Usually, the main stages of the analysis and Calculations are:

1. Calculation and verification of the system natural frequency: The subassemblies (winding stator, rotor stack with shaft etc.) model can be built and the natural frequencies and mode shapes can be calculated.
2. Electromagnetic model and force calculation: All the related dimensions, phase winding turns and the properties of all materials are modeled in a software package, for instance, in ANSYS, to calculate the flux linkage curves as a function of rotor position and phase current. Usually the two-dimensional electromagnetic finite element model is applied, perhaps with a correction factor for the three dimensional end effects. Based on the current and rotor position, both radial and tangential forces are calculated. The vibration and acoustic noise are determined based on the results of the finite element analysis.

Vibration Modes of All Laminations (M19) and All SMC Configurations

The vibration modes and resonant frequencies has been calculated with the aid of ANSYS commercial finite element package for the 6/4 machine shown in Figure 1.

The following assumptions are made in predicting the frequencies: (a) the stator yoke is a round rigid body; (b) the teeth and windings have no rigidity, so that their mass is attached to the yoke; (c) the periodic force waves with r th order are symmetrically exerted

on the stator yoke ring; (d) the only effects of all defects and notches is a reduction in the mass.

The following formulas (7) and (8) are used to predict the natural vibration frequencies for the force wave with r th order, where m is the equivalent mass per square meter (kg/m^2) on the cylindrical surface at the average yoke radius, which can be expressed as:

$$f_r = \frac{1}{2f} \sqrt{\frac{k_r}{m}} \quad \dots(7)$$

$$m = \frac{M_y}{2f R_{y(av)} L_{y(eff)}} \quad \dots(8)$$

and the equivalent spring stiffness coefficient per square meter k_r (N/m^3) on the cylindrical surface at average yoke radius (9) -(11),

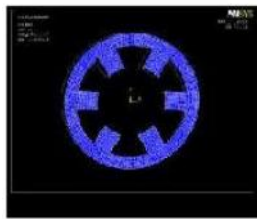
$$K = \begin{cases} \frac{E h_y}{R_{y(av)}^2} & \text{for } r = 0 \end{cases} \quad \dots(9)$$

$$\begin{cases} \frac{r^2 (r^2 - 1)^2}{r^2 + 1} \frac{E h^3}{12 R_{y(av)}^4} & \text{for } r \geq 2 \end{cases} \quad \dots(10)$$

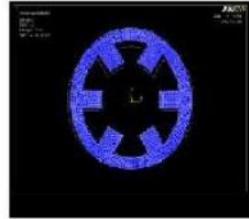
M_y is the yoke mass including stator windings and poles (kg); h_y is the yoke height in the radial direction (m); $R_{y(av)}$ is the average radius of yoke (m); $L_{y(eff)}$ is the effective length of yoke; k_D is the spring stiffness coefficient of the shock absorber under the motor. The resonant frequencies calculated for the two configurations viz., (i) All laminated sheet steels, (ii) All Soft Magnetic Composites (SMC) using structural finite element analysis are listed in Table 1.

This paper also considers the effects of the frame on the mode shapes and frequencies. A tight friction coupling between the laminations and frame is assumed.

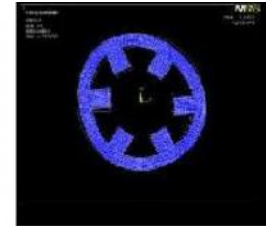
Figure 6: Vibration Modes of the Stator Laminations (M19) with Smooth Frame



a) Mode at 901.147HZ

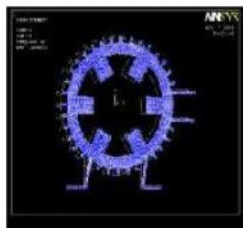


b) Mode at 2298 HZ

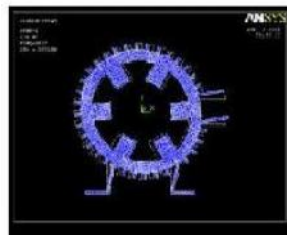


c) Mode at 4454HZ

Figure 7: Vibration Modes of the Stator Laminations (M19) with Ribbed Frame



a) Mode at 484HZ

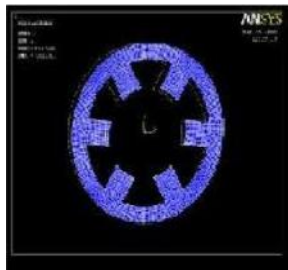


b) Mode at 1527HZ

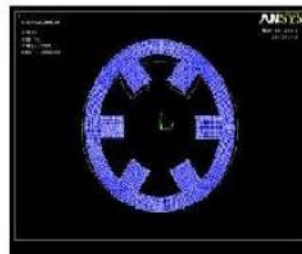


c) Mode at 1972HZ

Figure 8: Vibration Modes of the SMC Stator with Smooth Frame



a) Mode at 700



b) Mode at 1786



c) Mode at 3470

Figure 9: Vibration Modes of the SMC Stator with Ribbed Frame



a) Mode at 371



b) Mode at 1170



c) Mode at 1512

All SMC	a) 700	a) 371	329
	b) 1786	b) 1170	616
	c) 3470	c) 1512	1958
All M19	a) 901	a) 484	417
	b) 2298	b) 1527	771
	c) 4454	c) 1972	2482

Figures 5 and 6. Shows the effects of smooth frame and ribbed frame to the all laminations (M19) stator. Given the influence of the smooth frame and frame with ribs on the natural frequency, it is therefore of interest to examine the effects of the smooth frame and frame with ribs on the natural frequencies. Figures 7 and 8, summarizes the results for the case of a z-constrained vibration of a smooth frame and frame with ribs for all SMC configuration, the result showing that a gradual decrease (almost 45%) in the mode shape frequencies of frame with ribs. The overall vibration mode shape frequencies shows that the structural capability of configuration (ii) is better then when compared with configuration (i) in the high-speed aerospace applications. The Table 4 shows the comparison of smooth and ribbed frame with SMC and M19 materials.

CONCLUSION

In this paper an in-depth study of vibration modes of the stator of switched reluctance machine with two configurations viz., (i) All laminated sheet steels, (ii) All Soft Magnetic Composites (SMC) has been conducted. The study started with the laminations and SMCs with a smooth frame, and then extended as well to a ribbed frame. The studied result

shows that Mechanical characteristics of SRM viz., nodal temperature distributions at the different parts of the machine with SMC and M19 configurations, smooth stator frame and ribbed stator frame, 2D finite element analysis. Study has led to the SMC based switched reluctance motor configuration with ribs provision has better thermal behavior characteristic. The finite element analysis aided in the estimation of exact temperature distribution in the two motor configurations and their visualization. And gradual decrease (almost 45%) in the mode shape frequencies of frame with ribs. The considerable torque reduction in configuration (ii) is due to the poor permeability of soft magnetic composite material. On the other hand the structural capability of configuration (ii) is better when compared with configuration (i) in the high-speed aerospace applications regime. The finite element analysis aided in the estimation of temperature distribution and mode shape frequencies for the two motor configurations and in their visualization.

REFERENCES

1. Chin Y K, Nordlund E and Station D A (2003), "T Lumped-Circuit Model and Finite the 6th International Power Electronics Conference (IPEC), November, pp. 952-957, Singapore.
2. Colby R S, Mottier F and Acoustic T J E (1995), "Noise in a 4-Phase Switched Reluctance mo the 1995", *IEEE Industrial Application Society*, 30th IAS Annual Meeting, Vol. 1, October 8-12, pp. 441-447, Orlando, USA.
3. Holman J P (1976), *Heat Transfer*, McGraw Hill, USA.

-
4. Miller T J E (1993), "Switched Reluctance Motor and their Control", Oxford Unive. Press, London, UK.
 5. Persson M, Jansson P, Jack A G and Mecrow B C (1995), "Soft Mag Composite Materials –Use for Electrical International Machi Conference on Electrical Machines and Drive at Durham", September, England.
 6. Pillay P and Cai W (1999), "An Inve Motors", *IEEE Trans. on Ind. Appl.*, Vol. 35, No. 3, pp. 589-596.
 7. Radun A V (1992), "Powerdensity", High Switched Reluctance Motor Drive for Aerospace Applications", *IEEE Trans. Ind. Applicat.*, Vol. 28, No. 1, pp. 113-119.
 8. Hogan (2003), "The Latest Development in Soft ma from Hoganas Metal Powders".
 9. Srinivas K N and Arumugam R (2001), "Finite Element Analysis in Procof", The IEEE Region 10 Electrical and Electronics Technology Conference, pp. 819-824.
 10. Wu C Y and Pollock C (1995), "Analysis Noise and Vibration in the Switched Reluct an Applications", Vol. 31, No.1, pp. 91-98.
 11. Yongxiao C and Jianhua W (1997), "Frequencies of Stator of Stator", Proc. 8th Int. Conf. Electric Machines and Drives, pp. 81-85.